

---

## Direct Measurements of Terminal-Level Lifetime in Nd:YLF

The terminal-level lifetime of a four-level laser fundamentally affects its gain saturation performance since slow relaxation rates from this level can form a “bottleneck” when the saturating pulses are significantly shorter than the terminal-level lifetime. As a result, the terminal-level lifetime is an important design parameter in achieving maximum energy extraction from high-peak-power laser amplifiers and  $Q$ -switched oscillator systems.

Terminal-level lifetimes reported in the literature for even the most common laser media such as Nd:YAG differ by as much as several orders of magnitude;<sup>1–4</sup> references for Nd:YLF<sup>2,3</sup> are less common and subject to the same uncertainty.

For most solid-state laser materials, the terminal-level lifetime is dominated by nonradiative relaxation processes involving the emission or absorption of host material phonons. Closely spaced energy levels within a Stark manifold thermalize extremely rapidly ( $<10$  ps)<sup>5,6</sup> through nonradiative processes involving single phonons, while relaxation between different Stark manifolds proceeds at significantly slower rates since multiple phonons are required to bridge the typically larger intermanifold energy gaps. When the total multiphonon, nonradiative relaxation out of the terminal laser level manifold is much slower than the intramanifold thermalization, the distribution of population within the manifold can be treated as a system in quasi-thermal equilibrium and described by a Boltzmann distribution. For laser systems in which the terminal laser level contains a significant proportion of its thermalized manifold population, gain saturation properties are determined by both the relaxation rate of the entire manifold and the quasi-thermal occupation factor in the terminal laser level. The manifold relaxation rate, often characterized by its lifetime, determines whether any “bottlenecking” occurs, and the thermal occupation factor determines the degree to which accumulation of population in the terminal-level manifold reduces population inversion during lasing.

Measured lifetimes for other energy levels can yield relevant information since multiphonon nonradiative relaxation

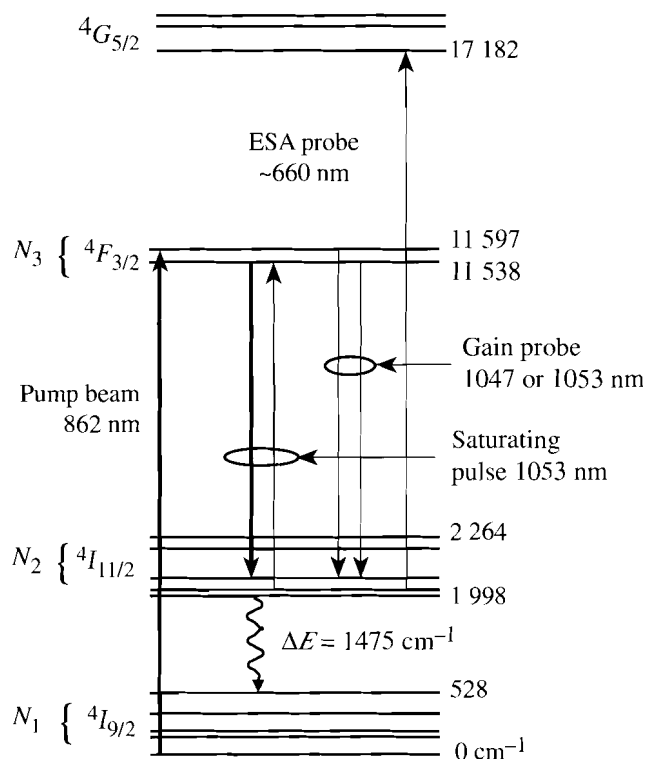
rates generally follow a phenomenological model<sup>7,8</sup> that depends only on temperature, energy gap to the next lower energy level, and a single phonon frequency. Measured relaxation rates for high-order phonon processes ( $n > 3$ ) substantially support this model;<sup>9,10</sup> however, it is generally invalid for low-order processes ( $n \leq 3$ ). Anomalies have also been observed in some materials<sup>8</sup> due to selection rules or when a high degree of resonance exists between an intermanifold energy gap and a sum of phonon energies corresponding to peaks in the host material’s phonon spectrum. In addition, significantly different lifetimes for nonradiative transitions covering nearly identical energy gaps have been reported for Nd:YAG<sup>3,11</sup> that suggest either a breakdown in the model or a dependence on the measurement technique.

Direct measurement of the  ${}^4I_{11/2}$  terminal-level relaxation is performed ideally under prototypical energy extraction conditions to ensure meaningful results. Sensitive and accurate measurement of the relaxation rate demands operating in a regime that clearly isolates the multiphonon nonradiative decay process from radiative processes. Saturating pulses substantially shorter than the terminal-level lifetime can yield a true impulse response that is easily analyzed without the need for deconvolving input beam pulse shapes or applying complicated models of the population dynamics. Any practical method should by design also minimize the amount of sample required and avoid nonlinear optical processes, such as self-focusing or self-phase modulation, that might damage the sample or otherwise introduce unquantifiable effects into the measurement.<sup>12</sup>

### Theory

Figure 62.31 represents the energy levels in Nd:YLF important to laser action. The  $1475\text{-cm}^{-1}$  energy gap<sup>13</sup> between the  ${}^4I_{11/2}$  terminal-level manifold and the  ${}^4I_{9/2}$  ground-state manifold is less than three times the phonon cutoff energy of  $566\text{ cm}^{-1}$  in YLF,<sup>14</sup> which places this nonradiative decay process near the limit of validity for the single-frequency model.

In this work, the  ${}^4F_{3/2}$  initial-laser-level manifold is pumped directly from the  ${}^4I_{9/2}$  ground-state manifold. Laser action at



E7446

Figure 62.31

Energy-level diagram for lasing in Nd:YLF. The  $4I_{9/2}$  ground state and  $4I_{11/2}$  terminal laser state are separated by a  $1475\text{-cm}^{-1}$  energy gap that is less than three times the maximum phonon energy in YLF<sup>14</sup> ( $\sim 566\text{ cm}^{-1}$ ). The thick upward (downward) arrow represents the pump (saturating pulse) laser transitions. The thin downward (upward) arrow represents the small-signal-gain (excited-state absorption) probe transitions.

the 1053-nm laser transition occurs between the lowest sub-level in the  $4F_{3/2}$  manifold and the second lowest level in the  $4I_{11/2}$  manifold. Since both the initial and terminal laser levels are strongly coupled to their respective Stark manifolds and each contains a substantial portion of its manifold's population, the relevant population dynamics are best described by rate equations for the total populations  $N_3$  and  $N_2$  of the initial ( $4F_{3/2}$ ) and terminal ( $4I_{11/2}$ ) laser-level manifolds, respectively,

$$\frac{dN_3(\bar{r}, t)}{dt} = W_{\text{pump}}(t) \cdot N_1(\bar{r}, t) - W_{\text{sat pulse}}(t) \times [f_3 N_3(\bar{r}, t) - f_2 N_2(\bar{r}, t)] - N_3(\bar{r}, t) / \tau_3, \quad (1a)$$

$$\frac{dN_2(\bar{r}, t)}{dt} = W_{\text{sat pulse}}(t) \times [f_3 N_3(\bar{r}, t) - f_2 N_2(\bar{r}, t)] - N_2(\bar{r}, t) / \tau_2, \quad (1b)$$

where  $W_{\text{pump}}$  and  $W_{\text{sat pulse}}$  are the radiative transition rates associated with the pump and saturating pulses, respectively, given by  $W(t) = I(t) \cdot \sigma / h\nu$ , where  $I(t)$  is the intensity,  $\sigma$  is the corresponding pump absorption or laser-stimulated emission cross section, and  $h\nu$  is the photon energy;  $\tau_3$  and  $\tau_2$  are the lifetimes of the initial and terminal-laser-level manifolds, respectively; and the thermal occupation factors of the actual Stark sublevels of the laser transition,  $f_3$  and  $f_2$ , are given by  $f_i = e^{-E_i/kT} / Z_i$ , where  $E_i$  is the energy of the sublevel within the manifold and  $Z_i$  is the partition function for the manifold. Given that no other energy levels accumulate significant populations, all relevant population dynamics are described by Eq. (1) plus the closure condition  $N_0 = N_1 + N_2 + N_3$ , where  $N_0$  is the doping concentration of the crystal and  $N_1$  is the total population of the  $4I_{9/2}$  ground-state manifold.

The rapid thermalization of the initial and terminal laser levels within their respective Stark manifolds can also be addressed in analytic solutions for laser-energy extraction performance<sup>15</sup> when saturating pulse lengths are short compared to the lifetime of the entire terminal-level manifold but long compared to the intramanifold thermalization processes. In a manner analogous to applying level degeneracy factors,<sup>16</sup> the expression for saturation fluence can be modified to include the thermal occupation factors  $F_{\text{sat}} = h\nu / (f_3 + f_2) \sigma_{\text{se}}$ , where  $\sigma_{\text{se}}$  is the spectroscopic stimulated emission cross-section. This expression reduces to the well-known value of  $F_{\text{sat}} = h\nu / \sigma_{\text{se}}$  for an ideal four-level system ( $f_3 = 1, f_2 = 0$ ), and  $F_{\text{sat}} = h\nu / 2\sigma_{\text{se}}$  for a three-level system ( $f_3 = 1, f_2 = 1$ ). Simple analytical models are inadequate for the intermediate case where laser pulse lengths are comparable to the terminal-laser-level manifold lifetime.

Figure 62.31 also shows small-signal-gain and excited-state absorption probes used in measuring the terminal-level lifetime. The small-signal-gain probe measures the population inversion  $\Delta N = f_3 N_3 - f_2 N_2$ , while the excited-state absorption probe monitors directly the population of the terminal manifold.<sup>12,17</sup> Assuming a plane-wave interaction, the time dependence of small-signal probe beams propagating in the  $x$  direction are determined by the population dynamics of the initial and terminal laser levels according to simple exponential growth and absorption laws

$$G_{\text{ss}}(t) = \exp \left\{ \int_{x=0}^L \Delta N(x,t) \sigma_{\text{se}} dx \right\}, \quad (2a)$$

$$T_{\text{ESA}}(t) = \exp \left\{ - \int_{x=0}^L f_2 N_2(x,t) \sigma_{\text{ESA}} dx \right\}, \quad (2b)$$

where  $\sigma_{\text{se}}$  and  $\sigma_{\text{ESA}}$  are the stimulated emission and excited-state absorption cross sections, respectively, and  $L$  is the sample thickness. The exponential arguments are integrated along the path traveled in the sample by the probe beams since the populations may vary spatially. Zero population in the  ${}^4G_{5/2}$  upper level of the excited-state absorption transition is assumed in Eq. (2b) for small probe signals.

After the initial-laser-level pumping has stopped and after an impulse-like saturating pulse has extracted stored energy at time  $t_0$ , Eqs. (1a) and (1b) become uncoupled differential equations with simple exponential solutions

$$N_3(x,t) = N_3(x,t_0) \cdot \exp \left[ -(t-t_0)/\tau_3 \right]$$

and

$$N_2(x,t) = N_2(x,t_0) \cdot \exp \left[ -(t-t_0)/\tau_2 \right],$$

where  $N_3(x,t_0)$  and  $N_2(x,t_0)$  are the population densities of the initial and terminal laser manifolds, respectively, left by the saturating pulse at  $t_0$ .

Substituting into Eq. (2) gives

$$G_{\text{ss}}(t > t_0) = G_{\text{final}} \cdot \exp \left\{ -\alpha_{\text{se}}(t_0) L \cdot e^{-(t-t_0)/\tau_2} \right\}, \quad (3a)$$

$$T_{\text{ESA}}(t > t_0) = \exp \left\{ -\alpha_{\text{ESA}}(t_0) L \cdot e^{-(t-t_0)/\tau_2} \right\}, \quad (3b)$$

where

$$\alpha_{\text{se}}(t_0) = \frac{1}{L} \int_{x=0}^L f_2 N_2(x,t_0) \sigma_{\text{se}} dx$$

and

$$\alpha_{\text{ESA}}(t_0) = \frac{1}{L} \int_{x=0}^L f_2 N_2(x,t_0) \sigma_{\text{ESA}} dx$$

represent the effective excited-state absorption coefficients for the small-signal probes at time  $t_0$ . Since the  ${}^4F_{3/2}$  initial laser-level lifetime is extremely long compared to the lower-level lifetime,<sup>6,18</sup> the upper-laser-level population can be taken as constant with a value  $N_3(t) \sim N_3(t_0)$ . The final small-signal gain after relaxation of the terminal laser level is given by

$$G_{\text{final}} = \exp \left\{ \int_{x=0}^L f_3 N_3(x,t_0) \sigma_{\text{se}} dx \right\}.$$

### Experimental Setup

Figure 62.32 illustrates the experimental setup. Thin Nd:YLF samples approximately 1 and 2 mm thick with nominal 1-at.-% doping concentrations are intracavity pumped directly into the  ${}^4F_{3/2}$  initial-laser-level manifold by a free-running, tunable Cr:LiSAF pulsed laser. The pump laser is tuned to the weak Nd:YLF absorption band at  $\sim 860$  nm using a birefringent tuning filter made from four crystalline quartz plates positioned at Brewster's angle. Horizontal polarization is further enforced by orienting the stronger  $\pi$ -polarization emission of the Cr:LiSAF rod to match the low-loss horizontal polarization of the Brewster tuning plates. The crystalline axis of the Nd:YLF sample is also horizontal to match the horizontal pump polarization with the stronger  $\pi$ -polarization absorption for Nd:YLF<sup>18</sup> ( $\alpha_{\text{max}} \approx 0.3 \text{ cm}^{-1}$ ). Operation in the TEM<sub>00</sub> mode is accomplished with an intracavity aperture in the nearly hemispherical resonator. Pump pulses with overall durations of approximately 70  $\mu\text{s}$  and numerous relaxation oscillations were obtained typically, as shown in Fig. 62.33. Uniform pumping is expected since the sample is optically thin at this wavelength. Furthermore, multiple-longitudinal-mode operation of the pump laser should smooth out any spatial hole burning that might occur early during the pump pulse. The diameter of the Nd:YLF sample's pumped region is approximately 1 mm in the vertical direction and elongated in the horizontal direction since it is also positioned at Brewster's angle inside the pump laser cavity to minimize reflection losses from the uncoated sample.

A saturating pulse is generated from an  $\sim 70$ -ps (FWHM) pulse picked from the output of a cw mode-locked Nd:YLF laser operating at 1053 nm and amplified to the millijoule regime in an unstable, regenerative ring amplifier.<sup>19</sup> The

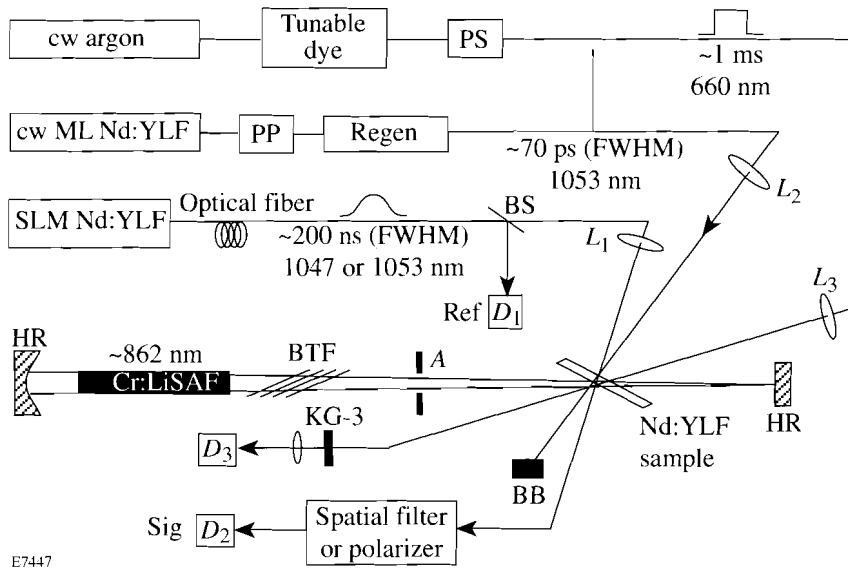
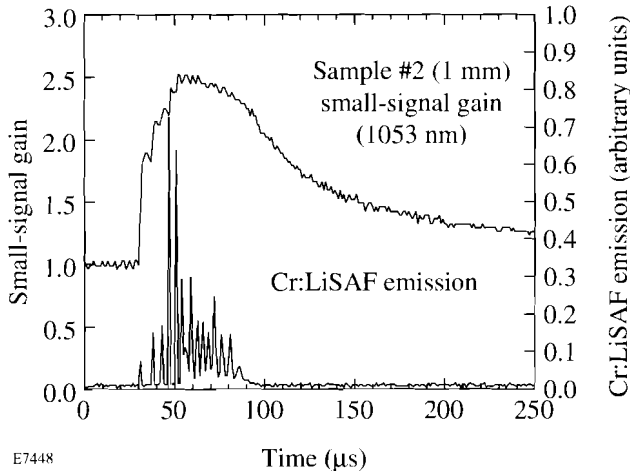


Figure 62.32

Experimental setup for measurement of terminal-level lifetimes;  $L_1$ ,  $L_2$ , and  $L_3$  = focusing lenses;  $D_1$ ,  $D_2$ , and  $D_3$  = fast silicon photodiodes; BTF = birefringent tuning filter; HR = high reflector mirrors; BB = beam block; BS = beam splitter; PP = pulse picker; PS = pulse slicer; SLM = single-longitudinal-mode laser; A = mode-controlling aperture; KG-3 = glass filter.

E7447



E7448

Figure 62.33

The time evolution of the Cr:LiSAF pump laser and the single-pass, small-signal gain through a pumped, 1-mm sample. Strong saturation of the pump absorption is observed after the first relaxation oscillation. The small-signal gain decays after termination of the pump pulse according to a double exponential characterized by an early time constant  $\tau = 30 \mu\text{s}$  and a long time constant  $\tau = 200 \mu\text{s}$ .

saturating pulse is cavity dumped from the regenerative amplifier and focused to  $\sim 400\text{-}\mu\text{m}$  diameter in the center of the sample's pumped region to achieve high saturation fluences. The polarization of the saturating pulse at the sample is vertical to align it with the 1053-nm ( $\sigma$ -polarization) axis of the Nd:YLF sample.

The small-signal-gain recovery of the Nd:YLF sample is measured using the fiber-coupled output of a  $Q$ -switched,

monomode Nd:YLF oscillator operating at either 1047 or 1053 nm. The approximately 200-ns FWHM, bell-shaped pulses are split into signal and reference beams that were measured by fast silicon photodiodes ( $\sim 150\text{-ps}$  rise time) using an HP 54720A fast digitizing oscilloscope (4 Gsamples/s, 1-GHz bandwidth). The signal-to-reference beam ratios were calculated for each shot to monitor the evolution of the single-pass, small-signal gain and then averaged over a number of shots. The small-signal-gain probe beam is focused to approximately a  $20\text{-}\mu\text{m}$  spot to spatially sample only the center of the saturated gain region. When using the 1053-nm probe beam, this spot was image relayed through a spatial filter to minimize light scattered from the saturating pulse into the solid angle of the signal-detector collection optics. For measurements with the 1047-nm probe beam, the probe beam polarization was orthogonal to the saturating pulse, and a thin-film polarizer was used to reject the scattered light. The actual single-pass, small-signal gain was obtained by removing passive effects, such as Fresnel reflections, and scattering in the sample measured by the signal beam when the sample was unpumped.

The transient excited-state absorption from the  $^4I_{11/2}$  terminal level was measured with a cw dye laser using DCM Special Dye (Lambda Physik LC 6501). The dye laser was pumped by a 5-W cw argon ion laser, and the output was tuned to 660.4 nm using a three-plate, quartz birefringent tuning filter. A mechanical shutter was used to gate 1-ms square pulses, both to reduce the average power incident on the fast silicon photodiode and to preserve its fast response time ( $\sim 150\text{-ps}$  rise time). A 2-mm-thick KG-3 Schott Glass filter was used to eliminate 1053-nm light scattered from the saturating pulse while passing the 660-nm probe beam. The

time-resolved measurements of optical transmission were averaged over a number of shots.

### Results and Discussion

Figure 62.33 illustrates a typical evolution of the single-pass, small-signal gain at 1053 nm achieved in a 1-mm-thick sample by the pump laser. Peak single-pass, small-signal gains greater than 2.5 were achieved in 1-mm-thick samples, and gains in excess of 4.0 in a 2-mm sample. The small-signal gain exhibits a double-exponential decay with lifetimes ( $\tau \approx 30 \mu\text{s}$  and  $\tau \approx 200 \mu\text{s}$ ) substantially shorter than published values for the fluorescence lifetime<sup>6,18</sup> for these low-doped crystals; however, even the fast component of this decay is still extremely long compared to the terminal-level lifetime. The reduced fluorescence lifetime appears to be related to the extremely high population inversion densities and visible fluorescence observed from the samples, which is likely the result of up-conversion processes promoted by the intense pumping. Background small-signal gain and excited-state absorption measurements taken without the saturating pulse present revealed no effect on laser-level population dynamics related to the intense pumping or the observed up-conversion processes on the time scale of the terminal-level lifetime.

Figure 62.34 illustrates a typical small-signal-gain ( $G_{ss}$ ) recovery measurement using the 1047-nm probe beam. The small-signal gain measured for a single pass of the probe beam through the pumped sample drops rapidly as the saturat-

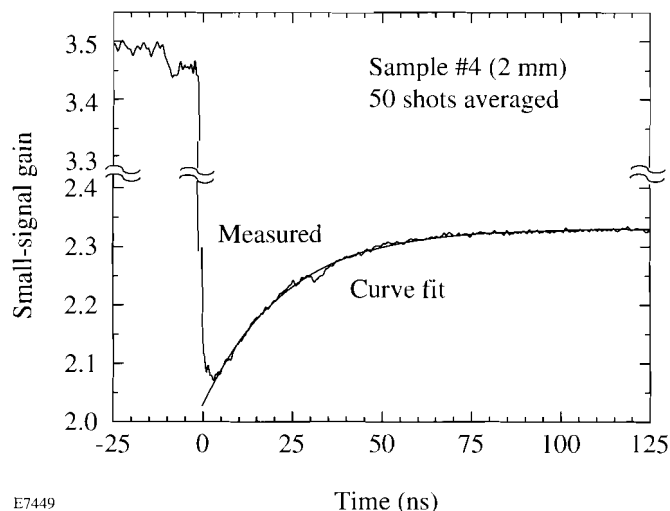


Figure 62.34

A typical small-signal-gain recovery measurement using the 1047-nm probe beam. The small-signal gain of a saturated sample (#4) recovers after passage of a short saturating pulse at  $t = 0$ . (Note the split vertical scale.) Curve fits using Eq. (3a) for  $t > 0$  for different samples are given in Table 62.IV.

ing pulse extracts stored energy at time  $t = 0$ . The small dip observed at  $t = -10$  ns is caused by a prepulse leaked one roundtrip before the regenerative amplifier is cavity dumped. The smooth recovery after  $t = 0$  to an asymptotic value caused by relaxation of the terminal laser level can clearly be seen along with a nonlinear exponential best fit to Eq. (3a). Table 62.IV presents average curve-fit values for the terminal-level lifetime of three different samples using both the 1047- and 1053-nm probe beams, as well as the standard deviation of the curve-fit values. No variations were observed for different positions in the samples measured, and excellent agreement is found from sample to sample.

Figure 62.35 displays a typical transient excited-state-absorption (ESA) measurement using another Nd:YLF sample. Larger transient ESA measurements were observed for  $\pi$ -polarized probe beams. The transmission through the pumped region of the sample is unity until the saturating pulse rapidly populates the terminal laser level at time  $t = 0$ . The observed transmission of the sample decreases rapidly and then returns to its equilibrium value on a time scale governed by the terminal-level lifetime. A nonlinear best fit to Eq. (3b) is also plotted. Again, evidence of a prepulse is observed at  $t = -10$  ns. Table 62.IV also includes curve-fit values for the terminal-level lifetime obtained from transient ESA measurements on several samples that are in excellent agreement with the values obtained from the small-signal-gain recovery measurements.

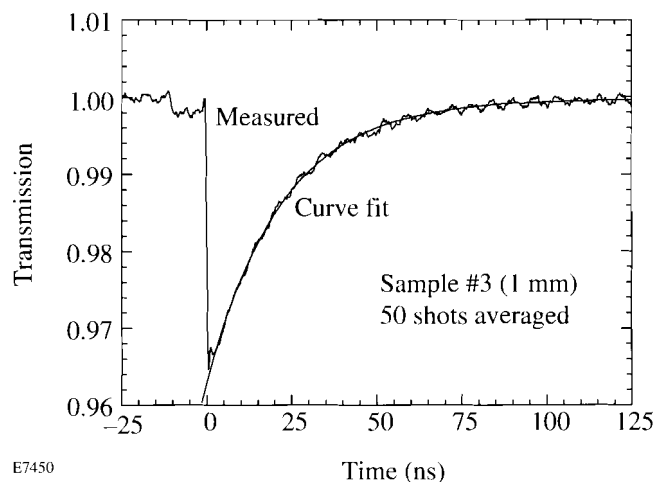


Figure 62.35

A typical ESA measurement in a different Nd:YLF sample (#3). Transient excited-state absorption from the terminal level occurs after passage of a short saturating pulse at  $t = 0$ . Curve fits using Eq. (3b) for  $t > 0$  for different samples are given in Table 62.IV.

Table 62.IV: Measured values for the terminal-level lifetime of four different Nd:YLF samples using small-signal-gain ( $G_{SS}$ ) recovery and transient excited-state absorption (ESA) methods are consistent within experimental accuracy.

Sample	Thickness (mm)	Lifetime (ns)	Standard Deviation (ns)	Method
1	1.015	21.9	$\pm 0.2$	1047-nm $G_{SS}$ recovery
2	1.100	21.9	$\pm 0.2$	1047-nm $G_{SS}$ recovery
		21.4	$\pm 0.4$	1053-nm $G_{SS}$ recovery
		21.8	$\pm 0.2$	transient ESA
3	1.435	21.4	$\pm 0.2$	transient ESA
4	2.230	21.3	$\pm 0.3$	1047-nm $G_{SS}$ recovery
		21.7	$\pm 0.7$	transient ESA

**Conclusions**

The terminal-level lifetime for Nd:YLF measured in this work is long compared to the pulse lengths encountered for mode-locked laser operation and amplification of up to nano-second pulses. In these cases, Nd:YLF must be treated as a three-level system amenable to standard Frantz-Nodvik gain saturation analysis with a modified expression for the saturation fluence that accounts for rapid thermalization of the initial and terminal laser levels within their respective Stark manifolds. Since common Q-switched laser pulse lengths are comparable to the terminal-laser-level lifetime measured in this work, simple analytical models are inadequate to account for terminal-level relaxation during amplification of such pulses, and numerical solutions are required to calculate energy-extraction performance.

**ACKNOWLEDGMENTS**

The authors wish to acknowledge Lightning Optical Corporation for providing the Nd:YLF samples. The authors also wish to thank S. A. Letzring for technical support related to high-speed instrumentation and electro-optic elements used throughout the experiments. This work was supported by the U.S. Department of Energy Office of Inertial Confinement Fusion under Cooperative Agreement No. DE-FC03-92SF19460 and the University of Rochester. The support of DOE does not constitute an endorsement by DOE of the views expressed in this article.

**REFERENCES**

1. F. E. Hovis *et al.*, IEEE J. Quantum Electron. **28**, 39 (1992).
2. K. Palomho *et al.*, in *OSA Proceedings on Advanced Solid-State Lasers, 1993*, edited by A. A. Pinto and T. Y. Fan (Optical Society of America, Washington, DC, 1993), Vol. 15, pp. 78–80.
3. C. Bibeau, S. A. Payne, and H. T. Powell, in *OSA Proceedings on Advanced Solid-State Lasers, 1994*, edited by T. Y. Fan and B. H. T.

Chai (Optical Society of America, Washington, DC, 1994), Vol. 20, pp. 74–76.

4. W. Koechner, *Solid-State Laser Engineering*, 2nd rev. and updated ed., Springer Series in Optical Sciences, Vol. 1 (Springer-Verlag, New York, 1988), p. 49.
5. T. Kushida, Phys. Rev. **185**, 500 (1969).
6. A. L. Harmer, A. Linz, and D. R. Gabbe, J. Phys. Chem. Solids **30**, 1483 (1969).
7. H. W. Moos, J. Lumin. **1,2**, 106 (1970).
8. L. A. Riseberg and M. J. Weber, in *Progress in Optics*, edited by E. Wolf (North-Holland, New York, 1976), Vol. XIV, pp. 91–159.
9. M. J. Weber, Phys. Rev. B **8**, 54 (1973).
10. H. P. Jentsen, Ph.D. thesis, Massachusetts Institute of Technology, 1971.
11. T. T. Basiev *et al.*, J. Lumin. **53**, 19 (1992).
12. N. E. Bykovskii *et al.*, Sov. J. Quantum Electron. **18**, 783 (1988).
13. A. A. S. da Gama *et al.*, J. Chem. Phys. **75**, 2583 (1981).
14. E. Schultheiss, A. Scharmann, and D. Schwabe, Phys. Stat. Sol. (b) **138**, 465 (1986).
15. L. M. Frantz and J. S. Nodvik, J. Appl. Phys. **34**, 2346 (1963).
16. A. E. Siegman, *Lasers* (University Science Books, Mill Valley, CA, 1986), pp. 153–157.
17. V. A. Sychugov and G. P. Shipulo, Sov. Phys. JETP **31**, 438 (1970).
18. J. R. Ryan and R. Beach, J. Opt. Soc. Am. B **9**, 1883 (1992).
19. D. Y. Park, W. Seka, Y. Lin, and D. L. Brown, in the *Proceedings of the International Conference on Lasers '89*, edited by D. G. Harris and T. M. Shay (STS Press, McLean, VA, 1990), pp. 449–456.